J. Fluid Mech. (1985), *vol.* 160, *pp.* 77–92
Printed in Great Britain

Space–time results for a separating turbulent boundary layer using a rapidly scanning laser anemometer

By B. CHEHROUDI† AND R. L. SIMPSON‡
Department of Civil and Mechanical Engineering, Southern Methodist University, Dallas, Texas 75275

(Received 8 November 1984)

A rapidly scanning one-velocity-component directionally sensitive fringe-type laser-Doppler anemometer which scans the measurement volume perpendicular to the optical axis of the transmitting optics was used to investigate the flow structure of the steady freestream separated turbulent boundary layer of Simpson, Chew & Shivaprasad (1981*a*). Space–time correlations were obtained for the first time in a separated turbulent boundary layer and showed that the integral lengthscale L_y for the large eddies grows in size towards detachment, although the ratio of this lengthscale to the boundary-layer thickness remains constant. Results also indicate local dependence of the backflow on the middle and outer regions of the boundary layer at a given instant in time.

1. Introduction

The problem of turbulent boundary-layer separation due to an adverse pressure gradient is important for the design of devices such as rocket nozzles, airfoils and helicopter blades, and the design of fluidic logic systems. Using multi-velocity-component directionally sensitive laser-anemometer systems, Simpson, Chew & Shivaprasad (1981*a*, *b*) and Shiloh, Shivaprasad & Simpson (1981) reported extensive experimental results for a nominally two-dimensional separating turbulent boundary layer with an airfoil-type freestream velocity distribution. They concluded that velocity fluctuations in the backflow region are large compared with the mean backflow, instantaneous velocity gradients are substantially different from the mean velocity gradient, and mixing-length and eddy-viscosity calculation models fail in the backflow region. They also suggested that the large-scaled eddies strongly influence the backflow locally.

If large-scaled eddies are largely responsible for the events in the backflow region, then more detailed information such as instantaneous velocity profiles and/or correlation measurements could be used to investigate this matter. A new rapidly scanning laser-Doppler anemometer (SLDA) developed by Chehroudi & Simpson (1984) is capable of measuring mean-velocity profiles, r.m.s. velocity fluctuations and the downstream–upstream intermittency factor γ_{pu} at scanning frequencies up to 59 Hz. In addition, measurements of 'almost' instantaneous velocity profiles are also possible if a sufficient data rate is available (Chehroudi 1983).

† Present address: Mechanical and Aerospace Engineering Department, Princeton University, Princeton, NJ 08544.
‡ Present address: The Department of Aerospace and Ocean Engineering, Virginia Polytechnic Institute and State University, Blacksburg, VA 24061.

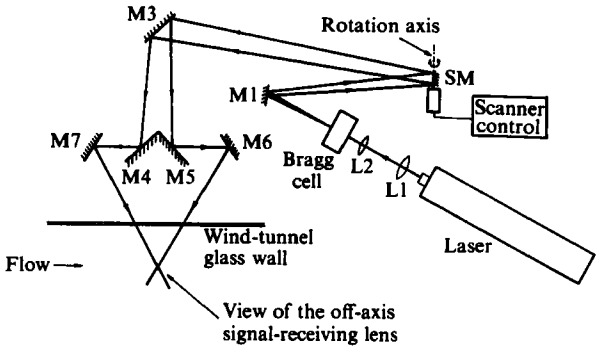

FIGURE 1. Schematic diagram of incident optics.

The work reported here provides new information concerning the flow structures in the separated region using this scanning LDA. Space–time correlation coefficients in the backflow region of a separated flow are reported and analysed for the first time.

2. Experimental equipment

2.1. *The wind tunnel and test flow*

The wind-tunnel geometry and the steady separated flow used here were the same as reported by Simpson *et al.* (1981*a*).

2.2. *Rapidly scanning laser-Doppler anemometer*

Figure 1 shows a top-view schematic of the transmitting optics of this one-velocity-component system. An argon ion, 5 W, Spectra Physics Model 164 laser with 514.5 nm wavelength is used. The laser beam passes through a lens combination L_1 and L_2 to decrease its diameter at the measurement point, and is split and frequency-shifted by a Bragg cell to have a directionally sensitive system. The outcoming beams from the Bragg cell are directed towards a rotationally oscillating scanner mirror SM by a small mirror M1. The beams are then reflected to the last-stage mirrors M5–M7 by a long fixed mirror M3. The measurement volume moves perpendicular to the plane of figure 1 as the scanner mirror SM oscillates. A linear scanning position versus time relation is used, and data are obtained as the measurement volume is scanned away from the wall.

The main idea in the design of the receiving optics is that one can detect the forward-scattered signals from the seed particles for any Y-position of the measurement volume throughout the scan range. Figure 2 shows the receiving-optics arrangement. Scattered light enters into the light-absorbing box through the first cylindrical lens CL_1. This lens focuses and enlarges the streamwise dimension of the measurement volume on the photomultiplier tube. The purpose of the second cylindrical lens CL_2 is to position the image of the probe volume on the PM tube throughout the scan range. A TSI Model 1980 counter-type LDA signal processor is used. For more information concerning the design of this scanning LDA and signal acquisition and processing see Chehroudi & Simpson (1984) and Chehroudi (1983).

Although a DOP aerosol seeder (Simpson *et al.* 1981*a*) and a polylatex-sphere solid-particle seeder (H. L. Seegmiller 1982 private communication, NASA–Ames Research Center) were tried, the following seeding method gave the best results. The

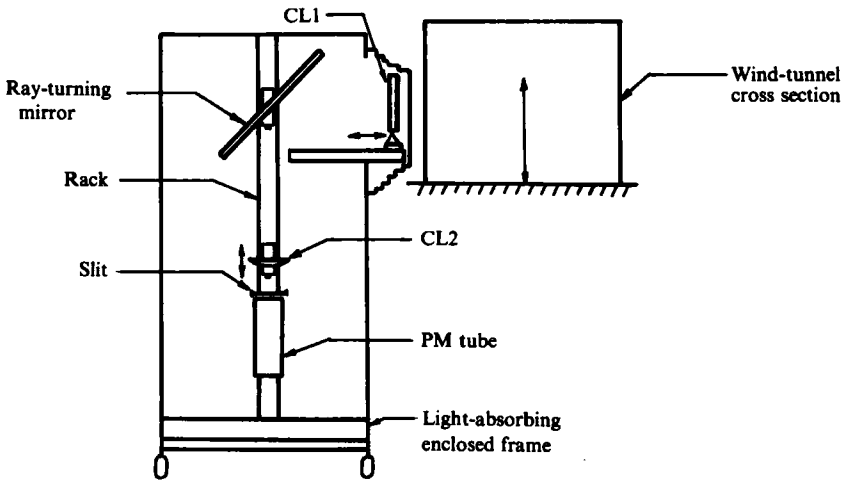

FIGURE 2. Schematic diagram of the receiving optics.

solid-particle seeder built at SMU (Chehroudi 1983) is similar in design to the Opto-Elektronische Instrumente (Karlsruhe, Germany) Model 101 solid-particle seeder, which uses talcum powder having particles greater than 1 μm. The talcum powder is pushed up inside a cylinder by an aluminium piston, and is scraped by a wire wheel at the opposite end of the cylinder. The upward speed of the piston can be varied to control the seeding rate. The outlet of the housing is directed to a conical manifold, which introduces the seeded air uniformly through a number of ports spaced uniformly across the test flow just upstream of the test-section leading edge.

3. Experimental results

3.1. *Mean r.m.s. velocities and the upstream–downstream intermittency*

Figures 3 and 4 show the mean and r.m.s. velocity fluctuations at four streamwise locations in the wind tunnel. In each case, the Y-scan range was divided into a chosen number of position bins, each ΔY in width. All of the validated measurements in a given ΔY-bin were used for computing the statistical parameters in that particular bin. The maximum number of validated measurements in each position bin did not exceed 500, and for this reason the sample size for comparative pointwise measurements, using the same scanning setup operated in a point-by-point measurement mode, was also chosen to be 500.

Figure 5 shows the intermittency factor γ_{pu}, the fraction of time flow is in the mainstream direction, for three streamwise stations. The intermittency factor is one throughout the boundary layer for $X = 317.5$ cm. The dip in γ_{pu} near the wall at the 436.9 cm location is a real effect as discussed by Simpson *et al.* (1981*a*), and not due to experimental uncertainty. If one divides the total number of validated velocity measurements in each position bin by the total time, T_{tb}, spent by the measurement volume in that bin for the entire record one will have an idea of the data rate throughout the boundary layer. Figure 6 shows the results for this parameter.

Reasonably good agreement between the pointwise and scanning LDA results is seen for the mean and r.m.s. velocities and the intermittency factor. The agreement is well within the ± 0.46 m s^{-1} uncertainty of the velocity, the ± 2 mm uncertainty

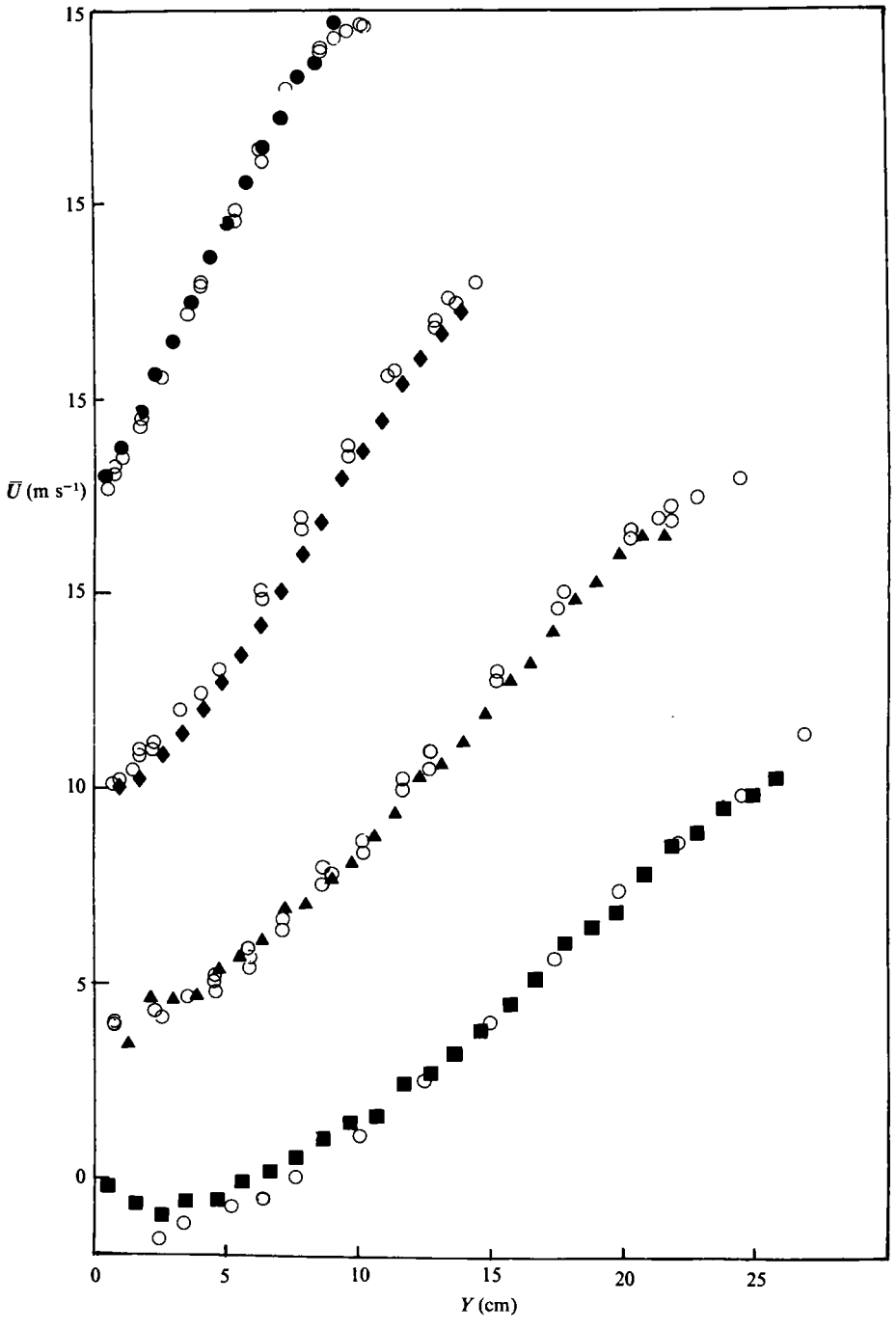

FIGURE 3. Mean velocity versus position at four different streamwise locations: ●, 317.5 cm; ◆, 355.6 cm; ▲, 396.2 cm; ■, 436.9 cm; ○ denotes corresponding pointwise measurements using the same scanning arrangement with sample size of 500.

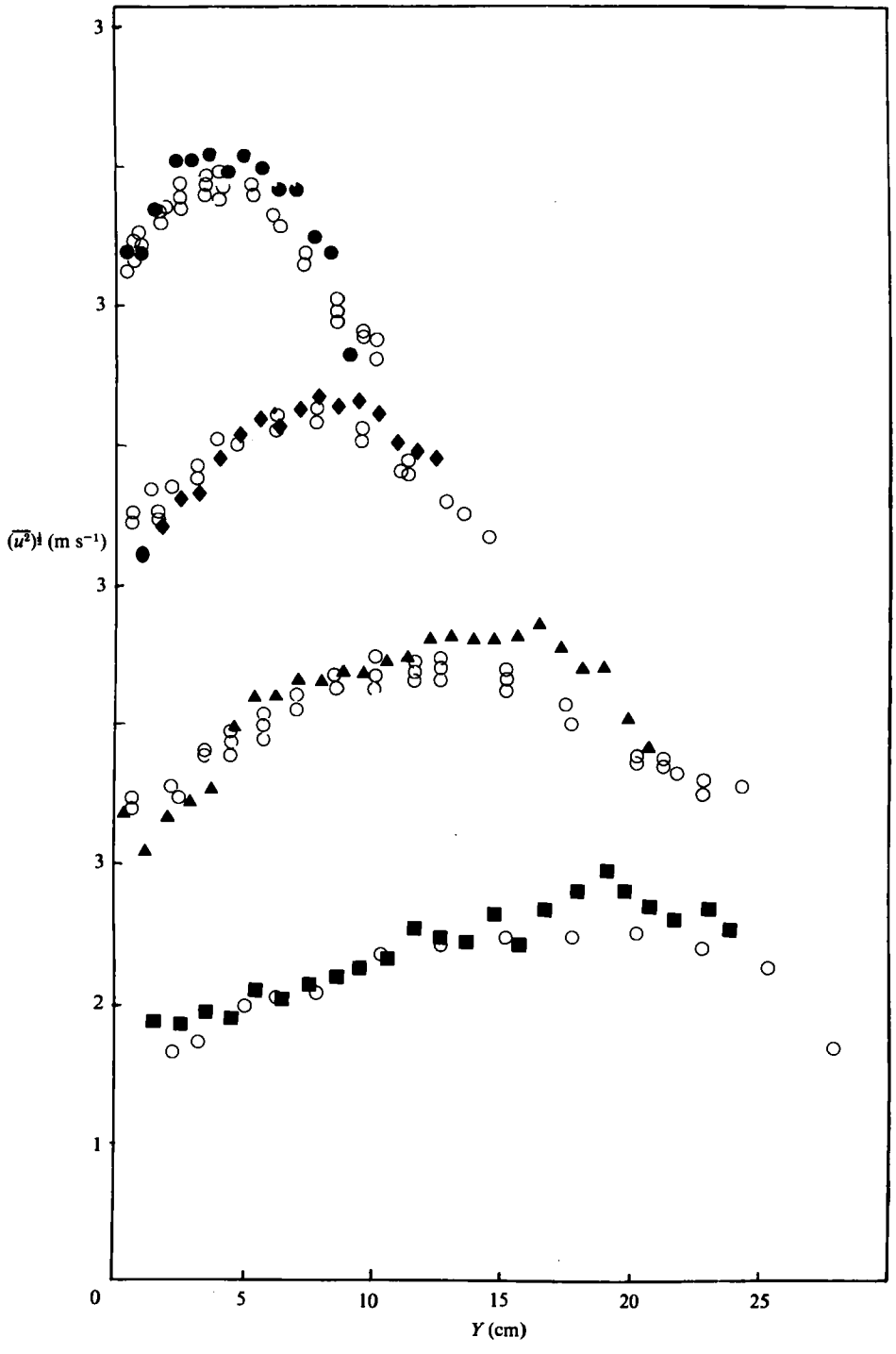

FIGURE 4. R.m.s. velocity fluctuations at four different streamwise locations. For legend see figure 3.

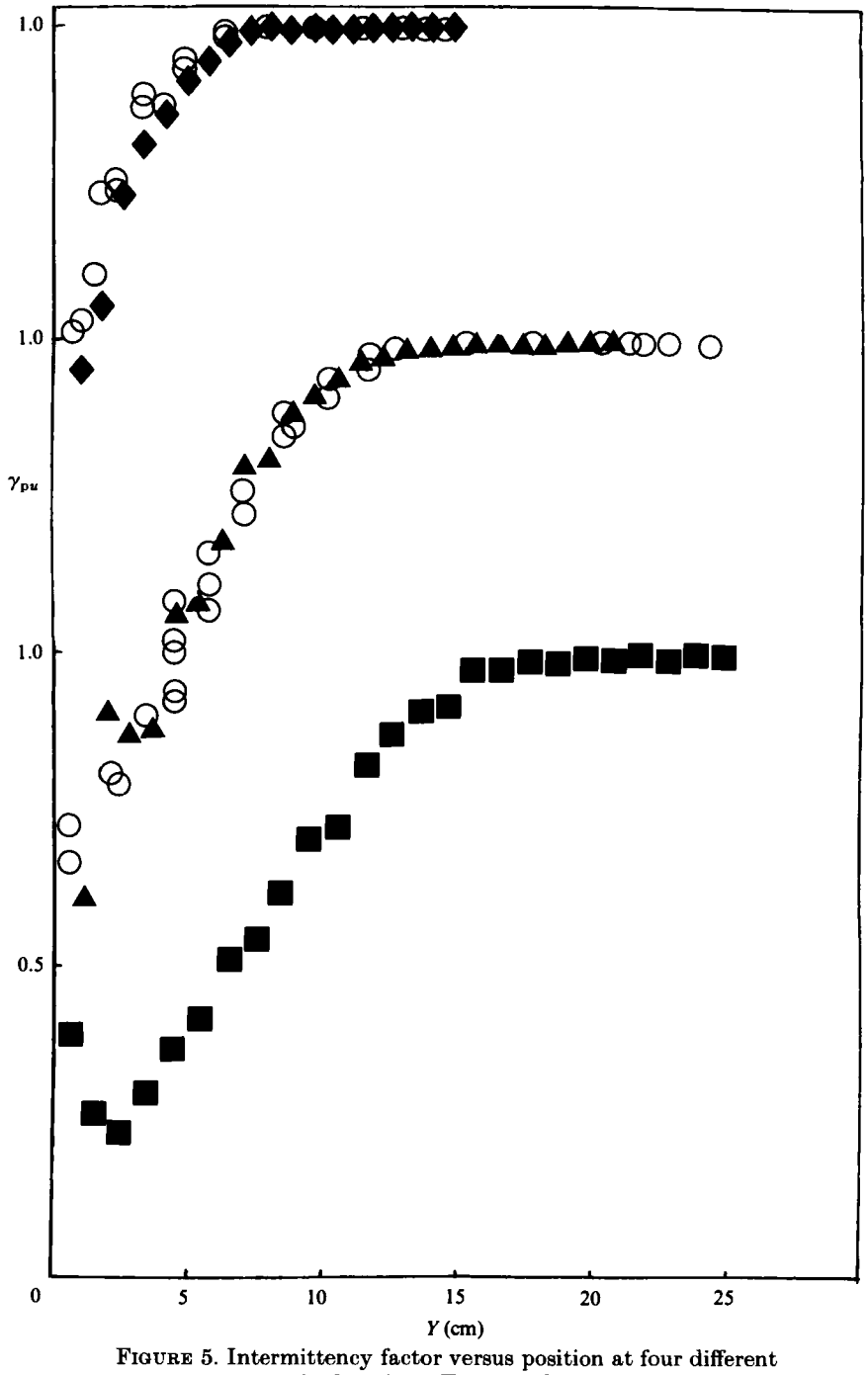

FIGURE 5. Intermittency factor versus position at four different streamwise locations. For legend see figure 3.

of the Y-position and the ± 0.07 uncertainty of γ_{pu} for the middle of the shear layer. Because of the variation of the vertical distance of the turbulent–non-turbulent interface and the fact that much of the talcum powder remains inside the boundary layer, the mean values are biased low near the edge of the boundary layer. Scatter

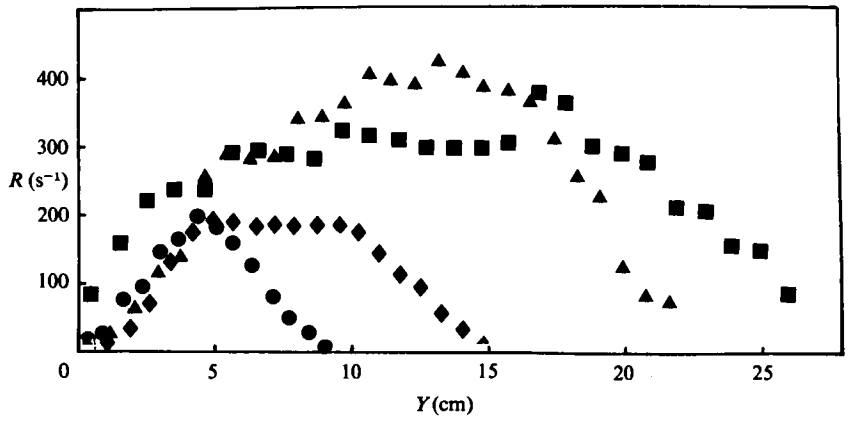

FIGURE 6. Number of samples per bin through boundary layer at four streamwise locations. $R \equiv$ (total number of samples)/(total record time for each bin).

in the r.m.s. values is attributed to the small sample size (500) for this calculation (Bates & Hughes 1976). A distinguishing feature of these results is that the mean and r.m.s. velocities and γ_{pu} are obtained in less than a minute of data acquisition at a high scan speed V_s of the measurement volume ($\sim$20 m s^{-1}).

3.2. *Space–time correlations*

Since the maximum number of validated measurements for a given scan in this work was not more than 20, there are insufficient data to obtain space–time correlations between discrete spatial positions. Hence the scan range was subdivided into several intervals. The correlations presented here are between two regions, each of finite dimension ΔY, rather than two points in the shear layer. At each streamwise location space–time correlations were evaluated between the first ΔY_1 interval at Y_1 near the wall and each of the ΔY_i intervals at Y_i throughout the shear layer.

The space–time correlation coefficient R_{uu} of the streamwise velocity fluctuations u was estimated according to

$$R_{uu}(Y_i - y_1, \tau) \equiv \frac{\Sigma u(Y_1 \pm \frac{1}{2}\Delta Y_1, t)\, u(Y_i \pm \frac{1}{2}\Delta Y_i, t+\tau)}{[\Sigma u^2(Y_1 \pm \frac{1}{2}\Delta Y_1, t)\, \Sigma u^2(Y_i \pm \frac{1}{2}\Delta Y_i, t+\tau)]^{\frac{1}{2}}}, \tag{1}$$

where the summation was taken over the entire record. Here $u(Y_i \pm \frac{1}{2}\Delta Y_i, t+\tau)$ means the velocity of fluctuation observed anywhere in the spatial interval

$$Y_i - \tfrac{1}{2}\Delta Y_i < Y < Y_i + \tfrac{1}{2}\Delta Y_i$$

at time $t+\tau$. The time delay was calculated from

$$\tau = \frac{m}{F_s} + \frac{Y_i - Y_1}{V_s}, \tag{2}$$

where m is the number of forward (positive) or backward (negative) cycles of time delay and F_s is the scan frequency. V_s is the upsweep scan velocity.

Figures 7–9 show $R_{uu}((Y_i - Y_1)/\delta, F_s\tau)$ for three streamwise locations: one downstream of the beginning of intermittent backflow but upstream of detachment, one just downstream of detachment and one far downstream of detachment. Note that

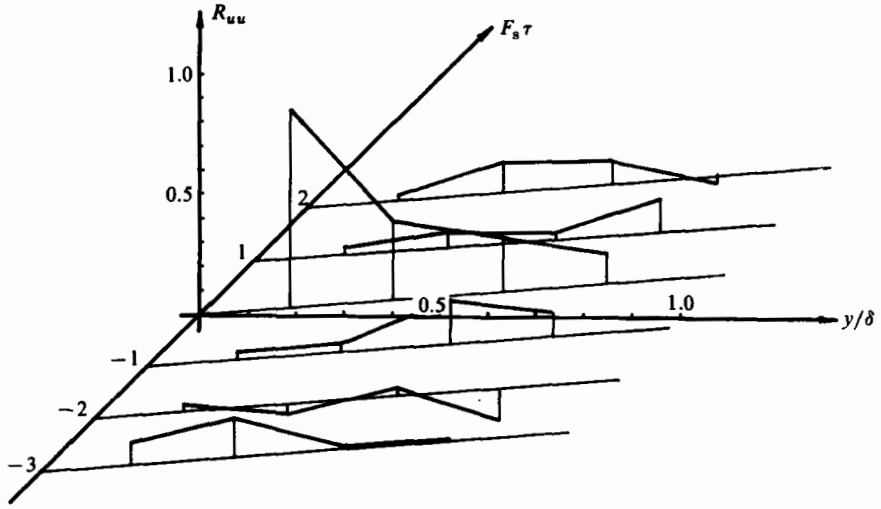

FIGURE 7. Space–time correlation coefficient between an interval near the wall and various intervals in the boundary layer. $X = 317.5$ cm, just downstream of the beginning of intermittent backflow; $\delta = 10$ cm. Scan frequency $F_s = 55.7$ Hz.

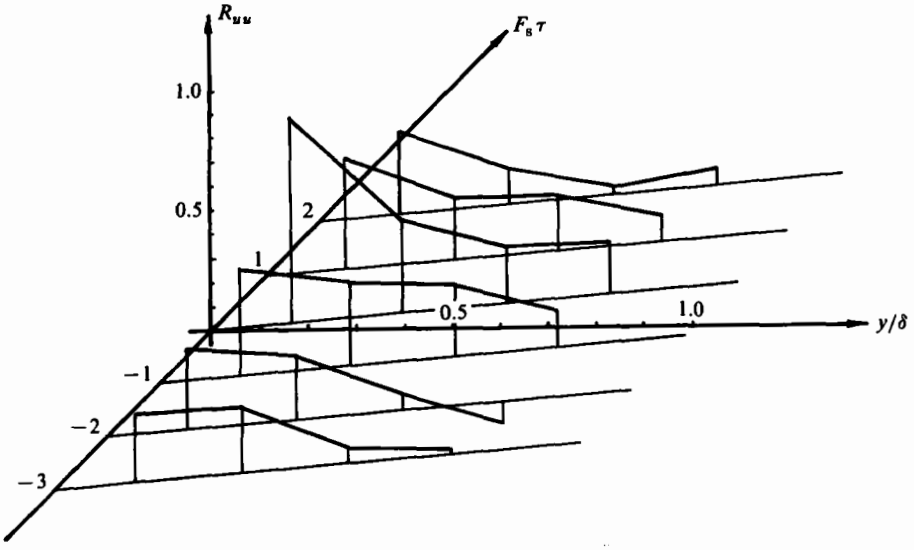

FIGURE 8. Space–time correlation coefficient between an interval near the wall and various intervals in the boundary layer. $X = 355.6$ cm, just downstream of detachment, $\gamma_{pu\,min} = 0.4$; $\delta = 15$ cm. Scan frequency $F_s = 56.6$ Hz.

the axes of these figures are normalized by the scan frequency and the boundary-layer thickness at that station. The space–time correlation for any region is represented by a vertical line.

The uncertainty of the space–time correlations was estimated by a comparison between autocorrelations from the scanning LDA velocity data and autocorrelations from a fixed-measurement-volume experiment at $y/\delta \approx 0.5$, where the maximum data rate was available. Departure of the scanning results from that of the fixed-measurement-volume data increases with the time delay. The uncertainty of

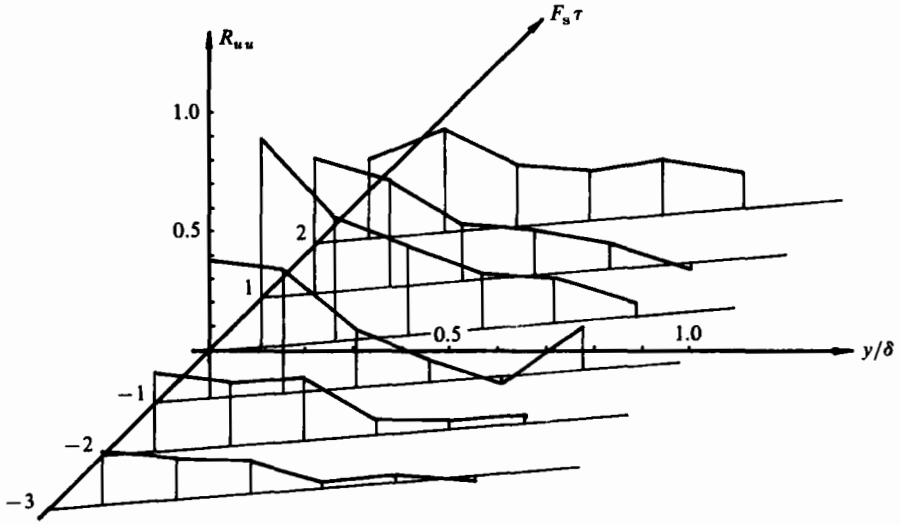

FIGURE 9. Space–time correlation coefficient between an interval near the wall and various intervals in the boundary layer. $X = 396.2$ cm, far downstream of detachment, $\gamma_{pu\ min} = 0.2$; $\delta_{0.99} = 24.5$ cm. Scan frequency $F_s = 58.6$ Hz.

the space–time correlations calculated from the scanning results was estimated to be ± 0.1 for the values shown in figures 7–9.

The space–time correlations for $y/\delta > 0.6$ are more uncertain for the following reasons. First, the data rate is low, as shown in figure 6, and consequently there are not sufficient points for proper convergence, since the total record time is also short. Secondly, owing to the time variation of the location of the turbulent–non-turbulent interface and the fact that the seeding particles tend to stay in the turbulent region, the values of correlation coefficients are higher there than correlation coefficients with both turbulent and non-turbulent flow. Finally, one should note that the correlation coefficients are between two ΔY spatial intervals of finite length rather than two points in the boundary layer.

3.3. *Quadrant analysis*

The fact that there may be a zero correlation coefficient for a long record time does not necessarily mean that there is no relationship between two flow regions during a short period. This motivated a quadrant analysis or correlation-diagram study of any possible dependency between the near-wall and outer regions of the separating shear layer.

As used here, a point in a quadrant plane shows the departure of the instantaneous streamwise velocity from the corresponding mean value $U - \overline{U} = u$ in a given spatial interval versus u for another spatial interval in the same scan of measurement volume. Figures 10–17 show the spatial intervals and typical results of the quadrant analysis using all scans in a data record for the streamwise location of 396.2 cm. The number of points in each quadrant is written in the corresponding quadrant.

4. Discussion

Qualitative investigations by Simpson *et al.* (1981*b*) showed that, for the case where the thickness of the backflow region is small compared with the turbulent shear-layer

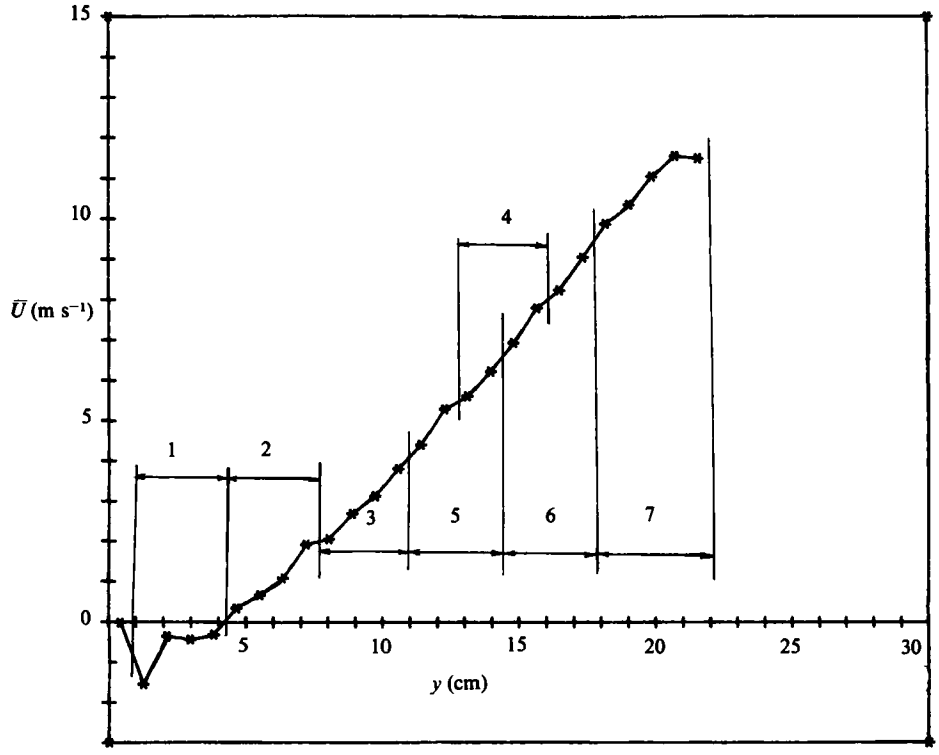

FIGURE 10. Mean velocity versus Y-position from scanning LDA data at $X = 396.2$ cm far downstream of detachment, showing spatial intervals used. u_1 and u_4 are fluctuations at a given scan in intervals 1 and 4 respectively. Scan frequency = 56.6 Hz.

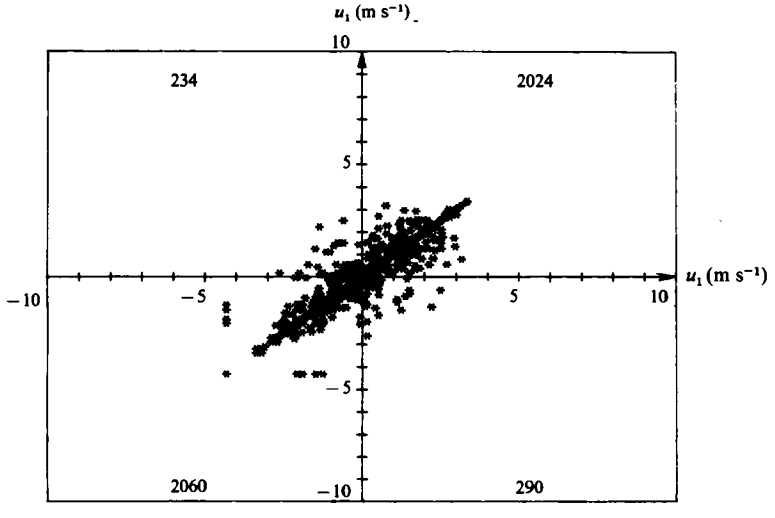

FIGURE 11. Quadrant analysis of u_1 fluctuation data in the first interval on the same scan. For intervals information see figure 10. $X = 396.2$ cm; $F_s = 56.6$ Hz; $R_{uu} = 0.869$. Number of points in each quadrant given in corresponding quadrant.

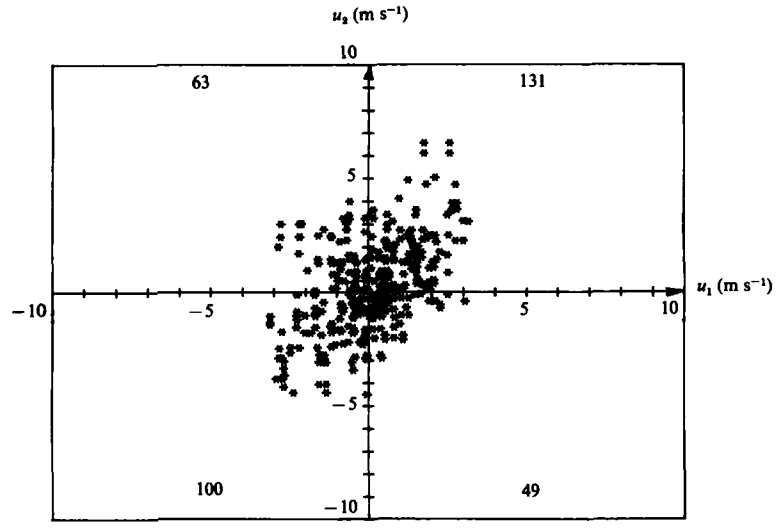

FIGURE 12. Quadrant analysis of u_1 and u_2 fluctuation data in adjacent near-wall spatial intervals from the same scan. For intervals information see figure 10. $X = 396.2$ cm; $F_s = 56.6$ Hz; $R_{uu} = 0.493$.

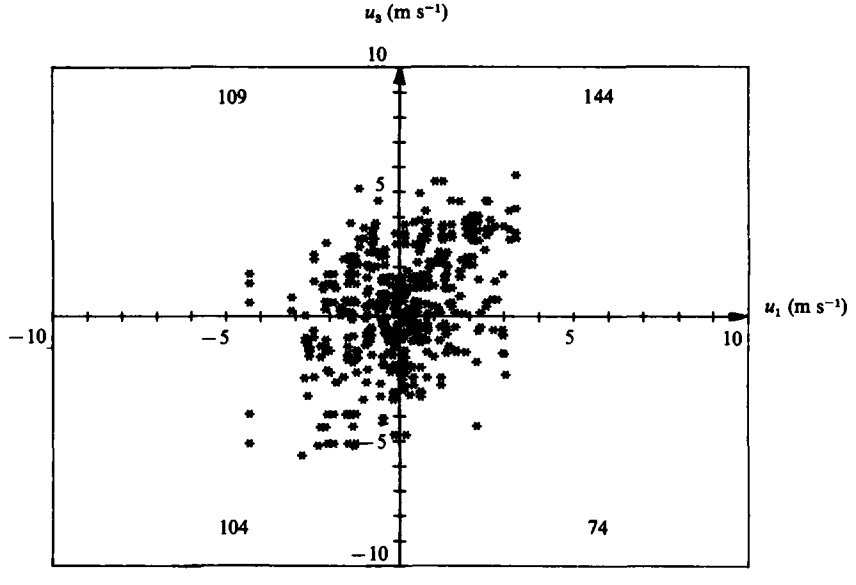

FIGURE 13. Quadrant analysis of u_1 and u_3 fluctuation data in spatial intervals 1 and 3 from the same scan. For intervals information see figure 10. $X = 396.2$ cm; $F_s = 56.6$ Hz; $R_{uu} = 0.374$.

thickness, the backflow region is strongly influenced locally by outer-region large-scale structures. The scanning LDA system used here can be useful for almost simultaneously examining flow structures across a shear layer, provided adequate data rates are achieved. The quadrant analyses and space–time correlations of scanning LDA measurements provide quantitative information on the nature of a detaching shear flow.

Space–time correlation coefficients for up to two cycles forward and three cycles backward time delay are reported here. As the flow goes towards detachment the

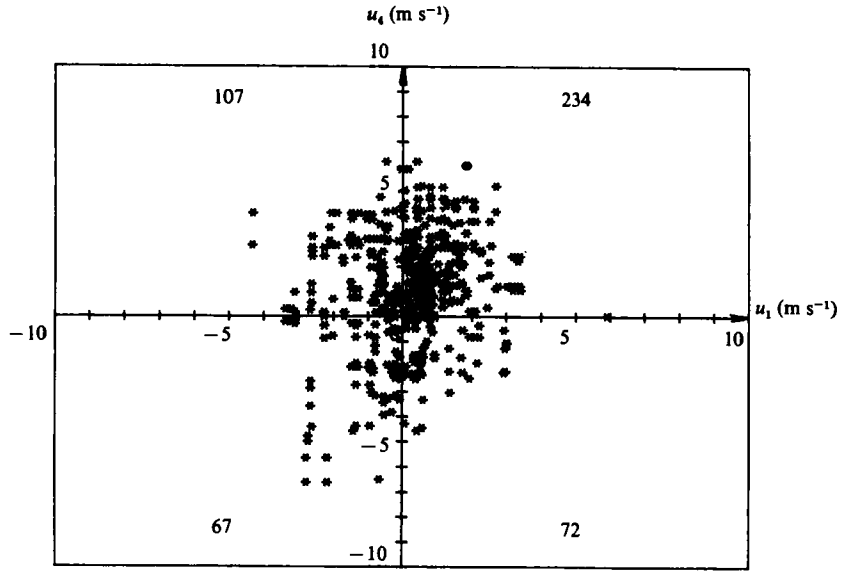

FIGURE 14. Quadrant analysis of u_1 and u_4 fluctuation data in spatial intervals 1 and 4 from the same scan. For intervals information see figure 10. $X = 396.6$ cm; $F_s = 56.6$ Hz; $R_{uu} = 0.184$.

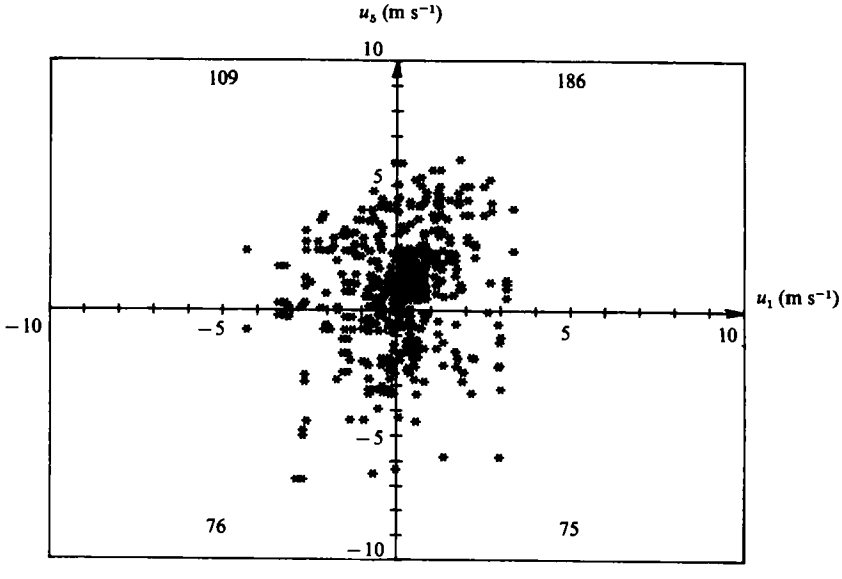

FIGURE 15. Quadrant analysis of u_1 and u_5 fluctuation data in intervals 1 and 5 from the same scan. For intervals information see figure 10. $X = 396.2$ cm; $F_s = 56.6$ Hz; $R_{uu} = 0.208$.

integral lengthscale $L_y = \int_0^\delta R_{uu}\,dY$ attains values of 3.55 ± 0.88 cm, 7.9 ± 1.30 cm and 8.18 ± 2.18 cm at $X = 317.5$ cm, 355.6 cm and 396.7 cm respectively. The ratio of the lengthscale to the corresponding boundary-layer thickness is about 0.35 ± 0.09. This means that the mean size of the eddy grows downstream.

Results from hot-wire anemometer spectra measurements (Chehroudi 1983) show that the non-dimensional parameter $U_\infty/\delta(n_{max})$ is approximately constant (≈ 4.71) for these streamwise locations. Hence n_{max} is the frequency corresponding to the

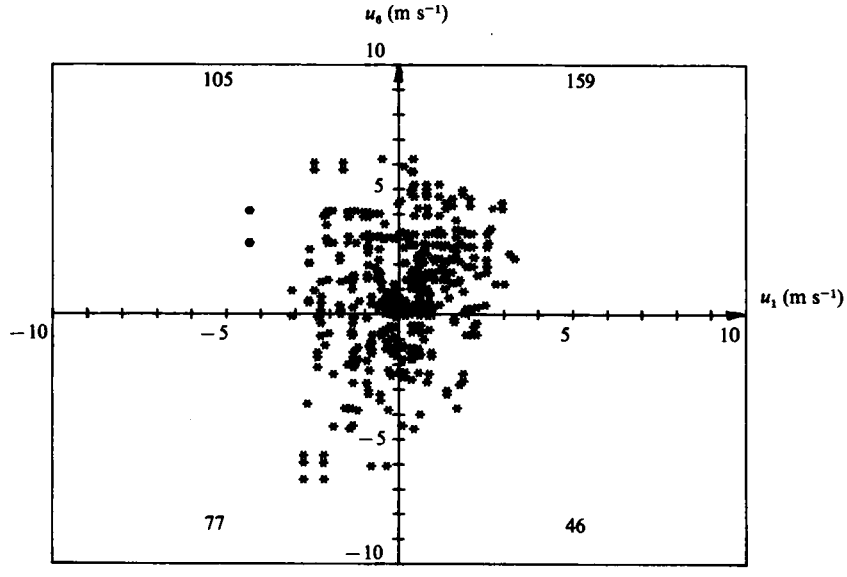

FIGURE 16. Quadrant analysis of u_1 and u_6 fluctuation data in spatial intervals 1 and 6 from the same scan. For intervals information see figure 10. $X = 396.2$ cm; $F_s = 56.6$ Hz; $R_{uu} = 0.205$.

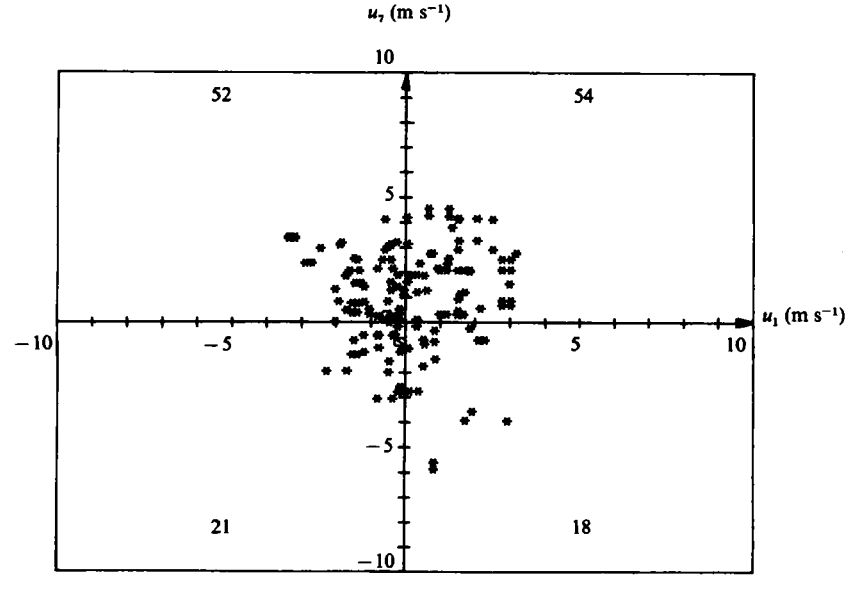

FIGURE 17. Quadrant analysis of u_1 and u_7 fluctuation data in spatial intervals 1 and 7 from the same scan. For intervals information see figure 10. $X = 396.2$ cm; $F_s = 56.6$ Hz; $R_{uu} = 0.041$.

maximum of the plots of 10 log $[nF(n)]$ versus frequency n at $y/\delta \approx 0.5$. Despite the limitations of the data, discussed in §3.2, one can see that the correlation between the near-wall region and the outer region decreases as the forward and/or backward delay time is increased. The correlation remains high for a longer time for the streamwise location of 396.2 cm, which is far downstream of detachment. This last

result is consistent with the fact that the frequency of the energy-containing eddies decreases in a downstream direction (Chehroudi 1983).

If $L_y(\tau)/\delta = \int_0^\delta R_{uu}(\tau)\,\mathrm{d}(y/\delta)$ for time delay τ, $L_y(\tau)/\delta$ appears to be approximately a function of $\tau n_{\max}$; for greater $|\tau|\,n_{\max}$, $L_y(\tau)/\delta$ decreases. For a given τ, figures 7–9 show less decay of R_{uu} for successive downstream locations since $|\tau|\,n_{\max}$ is less. If $R_{uu}(\tau)$ near the wall scales on $\tau n_{\max}$ then the timescale for the backflow is the local value of $1/n_{\max}$.

One distinguishing feature of the space–time correlation plots at streamwise locations of 317.5 cm and 355.5 cm is the approximate symmetry observed for forward or backward time delay. One can see in figure 9, which shows results far downstream of detachment, that the correlation coefficients for the forward time delay are higher than those for the corresponding backward time delay. One interpretation might be that the influence of the events happening near the wall in the backflow region on the outer region of the boundary layer is more than the influence of events occurring in the outer region on the near-wall region. To our knowledge, there are no other valid correlation-coefficient measurements available for the backflow region.

The interpretation of the quadrant analysis indicates that when flow is greater than the mean near the wall (ΔY-interval 1) then approximately $75 \pm 5\,\%$ of the time flow is greater than the corresponding mean values in the central region of the shear layer as well (figures 13, 14, 15). When the flow near the wall is less than the mean (larger backflow) then about $60 \pm 5\,\%$ of the time flow is greater than the mean in the outer region. One can reverse the viewpoint: given that the flow is greater than the mean in the outer region then $64 \pm 5\,\%$ of the time the flow is more positive than the mean near the wall. The flow near the wall and the flow in the middle and outer regions are simultaneously more positive than the mean or more negative than the mean $62 \pm 5\,\%$ of the time. These results indicate that there is substantially greater than $50\,\%$ probability that velocity fluctuations in the backflow and fluctuations in the middle and outer boundary layer have the same sign. This indicates that the flow structures in these regions are more than randomly related to one another.

Although the scanning LDA data rate was not sufficient to produce a large number of detailed velocity profiles from successive scans, figure 18 shows sample profiles for four successive scans. At this streamwise location, $n_{\max} = 8$ Hz, so on the average there were about 7 scans through each large-scaled structure as it passed downstream. The first scan shows a few positions near the wall where the velocity is high and the outer region where the velocity is lower than the mean velocity. On the very next scan negative velocities near the wall appear and more positive velocities occur near the middle of the flow. On the next two scans it appears that the velocity maximum moves closer to the wall. Although there are insufficient data points for each scan to be sure that this is the case, figure 18 shows the merit of examining 'almost' instantaneous velocity profiles to learn more about the flow structure.

5. Conclusions and recommendations

Space–time correlations indicate that the near-wall and outer regions of the separating boundary layer remain correlated for longer times as the flow proceeds downstream with a larger backflow region. A quadrant analysis downstream of the detachment point indicates that when the flow is greater than the mean in the outer region, then it is most probably greater than the mean near the wall too, and *vice versa*, which indicates some degree of coherence between those two regions.

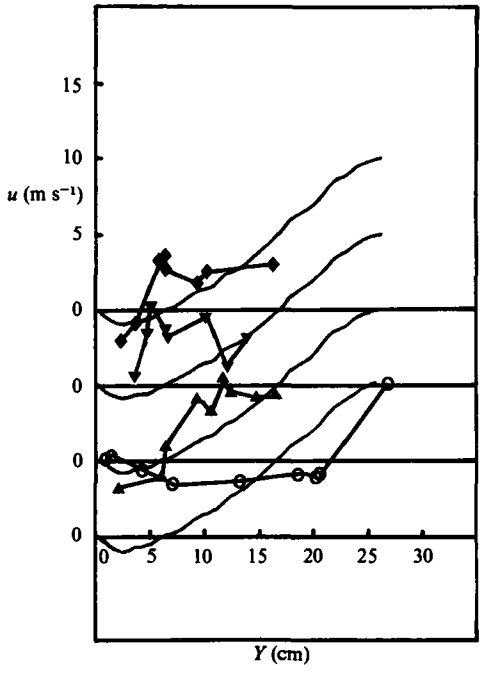

FIGURE 18. Instantaneous velocity profiles for four consecutive scans far downstream of detachment, starting from the lowest profile. $X = 436.6$ cm; $F_s = 58.2$ Hz. Mean-velocity profile at this location given by smooth curve. Data connected by straight lines for visual aid only. Note displaced ordinates.

In effect, the data and results presented here support the idea that the flow in the backflow region of a separating turbulent boundary layer is substantially related to the local outer-region flow at a given instant. As suggested by the experiments and discussion of Simpson *et al.* (1981*b*), the small mean backflow must not originate from far downstream in this flow, but appears to be supplied intermittently by large-scale outer-region structures of the order of δ in height and width, either by fluid motions towards the wall or by instantaneous streamwise pressure gradients set up by these structures. The smoke-wire flow-visualization results of Wei & Sato (1984) support this idea. This dependence of the backflow on the local outer-region flow means that separated flows of this type are not strongly dependent on the far-downstream turbulence structure and that a marching type of calculation method for the velocity field is possible.

'Almost' instantaneous velocity profiles are possible if a higher LDA rate could be achieved. This will be possible with an improved seeding technique and a LDA signal processor that can handle low signal-to-noise ratio signals.

This work was supported by the U.S. Office of Naval Research under contracts N00014-79-C-0277 and N00014-82-K-0554. The authors appreciate this support and the initial development work of the scanning LDA by Dr Klara Shiloh, now at the Israel Atomic Energy Commission. Dr Y.-T. Chew made several helpful suggestions about the manuscript.

REFERENCES

BATES, C. J. & HUGHES, T. D. 1976 *J. Phys.* E: *Sci. Instrum.* **9**, 955–958.

CHEHROUDI, B. 1983 Ph.D. dissertation, Dept Civ. Mech. Engng, Southern Methodist University, Dallas.

CHEHROUDI, B. & SIMPSON, R. L. 1984 *J. Phys.* E: *Sci. Instrum.* **17**, 131–136.

SHILOH, K., SHIVAPRASAD, B. G. & SIMPSON, R. L. 1981 *J. Fluid Mech.* **113**, 75–90.

SIMPSON, R. L., CHEW, Y.-T. & SHIVAPRASAD, B. G. 1981*a* *J. Fluid Mech.* **113**, 23–51.

SIMPSON, R. L., CHEW, Y.-T. & SHIVAPRASAD, B. G. 1981*b* *J. Fluid Mech.* **113**, 53–73.

WEI, Q.-D. & SATO, H. 1984 *J. Fluid Mech.* **143**, 153–172.